Indian Statistical Institute

ISI Digital Commons

Journal Articles | Scholarly Publications

6-1-2020

Emergence of bursting in a network of memory dependent excitable and spiking leech-heart neurons

Sanjeev Kumar Sharma
Indian Institute of Technology (Indian School of Mines), Dhanbad

Argha Mondal
University of Washington

Arnab Mondal
Indian Institute of Technology (Indian School of Mines), Dhanbad

Ranjit Kumar Upadhyay
Indian Institute of Technology (Indian School of Mines), Dhanbad

Chittaranjan Hens
Indian Statistical Institute, Kolkata

Follow this and additional works at: https://digitalcommons.isical.ac.in/journal-articles

Recommended Citation

Sharma, Sanjeev Kumar; Mondal, Argha; Mondal, Arnab; Upadhyay, Ranjit Kumar; and Hens, Chittaranjan, "Emergence of bursting in a network of memory dependent excitable and spiking leech-heart neurons" (2020). *Journal Articles*. 261.
https://digitalcommons.isical.ac.in/journal-articles/261

This Research Article is brought to you for free and open access by the Scholarly Publications at ISI Digital Commons. It has been accepted for inclusion in Journal Articles by an authorized administrator of ISI Digital Commons. For more information, please contact ksatpathy@gmail.com.

INTERFACE

royalsocietypublishing.org/journal/rsif

Research

Cite this article: Sharma SK, Mondal A, Mondal A, Upadhyay RK, Hens C. 2020 Emergence of bursting in a network of memory dependent excitable and spiking leech-heart neurons. *J. R. Soc. Interface* **17**: 20190859.
http://dx.doi.org/10.1098/rsif.2019.0859

Received: 16 December 2019
Accepted: 2 June 2020

Subject Category:
Life Sciences–Mathematics interface

Subject Areas:
biomathematics

Keywords:
excitable neuron model, fractional dynamics, stability, spiking–bursting, synchronization networks

Author for correspondence:
Argha Mondal
e-mail: arghamondalb1@gmail.com

†These authors contributed equally to this study.

Downloaded from https://royalsocietypublishing.org/ on 23 May 2022

Emergence of bursting in a network of memory dependent excitable and spiking leech-heart neurons

Sanjeev Kumar Sharma[1,†], Argha Mondal[2,3,†], Arnab Mondal[1], Ranjit Kumar Upadhyay[1] and Chittaranjan Hens[3]

[1]Department of Mathematics and Computing, Indian Institute of Technology (Indian School of Mines), Dhanbad 826004, India
[2]Computational Neuroscience Center, University of Washington, Seattle, WA, USA
[3]Physics and Applied Mathematics Unit, Indian Statistical Institute, BT Road, Kolkata 700108, India

SKS, 0000-0003-4807-8010; AM, 0000-0001-5540-8845; AM(Arnab Mondal), 0000-0002-8254-0590; RKU, 0000-0002-1210-7804; CH, 0000-0003-1971-089X

Excitable cells often produce different oscillatory activities that help us to understand the transmitting and processing of signals in the neural system. The diverse excitabilities of an individual neuron can be reproduced by a fractional-order biophysical model that preserves several previous memory effects. However, it is not completely clear to what extent the fractional-order dynamics changes the firing properties of excitable cells. In this article, we investigate the alternation of spiking and bursting phenomena of an uncoupled and coupled fractional leech-heart (L-H) neurons. We show that a complete graph of heterogeneous de-synchronized neurons in the backdrop of diverse memory settings (a mixture of integer and fractional exponents) can eventually lead to bursting with the formation of cluster synchronization over a certain threshold of coupling strength, however, the uncoupled L-H neurons cannot reveal bursting dynamics. Using the stability analysis in fractional domain, we demarcate the parameter space where the quiescent or steady-state emerges in uncoupled L-H neuron. Finally, a reduced-order model is introduced to capture the activities of the large network of fractional-order model neurons.

1. Introduction

Diverse neuronal responses in excitable cells can be triggered by injected stimulus current [1–5]. For instance, recurrent firing activities as spike trains, sequence of regular or chaotic bursting or mixed-mode type of oscillations may emerge in a single neuron. In particular, the activation property of slow (fast) potassium (sodium) ion channels or excitability encoded in a neuron determines these firing activities [3–5]. However, a complete description of firing patterns cannot be captured from a single neuron or group of neurons. This is a fundamental challenge in dynamical system theory as the mode transition across different firing patterns or emergence of scale invariance in membrane potential is always restricted [3,4,6] due to the limited access of parameter space in neuronal dynamics. To overcome these challenges, recently researchers have focused on fractional-order dynamics (FOD) [7–13] of neuronal models that can easily mimic (depending on fractional exponents) a wide range of electrical activities [14–17] or multiple timescale dynamics [18]. On the other hand, the firing rates of neocortical pyramidal neurons in the presence of applied sinusoidal stimulus current [19], several activities of potassium/sodium ion channels in conductance-based Hodgkin–Huxley or leaky integrate-and-fire model [18,20,21] may reflect scale-invariant power-law dynamics. All these above-mentioned features (complex firing patterns and emergence of scale-free distribution of ionic activities) can be easily explained in the light of fractional calculus connected to dynamics of neurons [17]. The intrinsic properties of fractional calculus is related to the capacity of

THE ROYAL SOCIETY PUBLISHING

© 2020 The Author(s) Published by the Royal Society. All rights reserved.

Downloaded from https://royalsocietypublishing.org/ on 23 May 2022

memory storage having long-range correlation which is significantly shifted from Markov process [22–25]. Note that FOD has a wide area of applications ranging from tissue engineering [24,26], diffusion process [27–32], networks [33] to the vestibular oculomotor system [34] and fly motion of sensitive neurons H1 [35,36]. It can be used as a powerful tool in understanding the mechanism of synapses [36] and geometrical properties of excitabilities of cells [34,37] and biophysical models [38–41]. Different types of biophysical models have various neurocomputational features. This type of work (based on FOD) determines basic functioning of the excitable cells when they are single or in a network architecture.

However, a detailed investigation on complex firing patterns emerging from the mixture of coupled heterogeneous fractional-order neurons are completely missing to the best of our knowledge. More precisely, we investigate the emergence of regular and recurrent bursting in a mixed population of fractional-order neurons in which a certain percentage of neurons are in silent state or follow subthreshold oscillations, whereas the rest show tonic spiking or periodic bursting. Note that, bursting is an alternation between repetitive spiking and quiescent states or subthreshold oscillations commonly found in neural system and worked as central pattern generators [42] also observed in pathological brain states [43], such as during epileptic seizures [43–45] and also in Josephson junctions [46]. These mixed type of neurons connecting in a network may exchange information (for instance, molecules passing through the sodium channel) via diffusive interaction.

The pertinent challenge that we would like to explore is the exploitation of the parameter space in such a way that total population within a complete graph will reflect recurrent firing or bursting, avoiding quiescent or steady states of uncoupled neurons. This article unfolds two important aspects of a collection of fractional-order neuronal dynamics: (i) how storage capacity/memory (the fractional parameter) determines the firing and quiescent activities of neuron or group of neurons and (ii) how such mixed population fire with multiple spikes in a single burst and avoids extinction in temporal domains over a certain coupling strength.

This is really a challenging but interesting task never explored before. As a paradigmatic neuronal dynamics, we use the electrical activities of leech-heart (L-H) interneuron model [47–50] as the nodes of the graph (see §2 and 3 for model description and stability). It is a biophysically plausible and computationally efficient mathematical model already established in previous studies. Note that the intrinsic parameter of each node in the network will be same; however, they change their dynamical features in the presence of fractional parameters. The fractional-order L-H model generates a wide range of oscillations with varying, α in (0, 1] while other parameters are fixed at their base values that can never be produced in a classical-order model. We have used history effects to shift the electrical activities towards steady state ($\alpha < 1$) from its original classical order domain ($\alpha = 1$) (see §4). The results suggest that diverse oscillations can be emerged due to the effects of memory properties of the FOD and interactions of the ionic currents [15,20]. In §5, we describe the network dynamics of the complex firing pattern in details. We will also show that the entire network fires with burst by forming cluster synchronization in which neurons within a subpopulation oscillate synchronously. We explore a semi-analytical description of a reduced-order model which can clearly mimic the collective features of globally connected L-H neurons in the backdrop of diverse memory settings. This type of study is important as different states of connected neurons (silent and oscillatory nodes) coexist in the same network and they fire together for a certain time and coupling strength.

2. Formulation of uncoupled fractional-order leech-heart interneuron model

The classical L-H interneuron model is described for its different electrical activities [47–50] in a wide range of interesting parameters that control the L-H cells. We consider the equations of motion of the L-H interneuron model for a commensurate fractional-order system as follows:

$$\left.\begin{aligned} \frac{\mathrm{d}^\alpha v}{\mathrm{d}t^\alpha} &= -2[30m^2(v+0.07)+8(v+0.046)+200h \\ &\quad (v-0.045)g^3(a_1,\ b_1,\ v)] = f_1(v,h,m), \\ \frac{\mathrm{d}^\alpha h}{\mathrm{d}t^\alpha} &= 24.69[g(a_2,\ b_2,\ v)-h] = f_2(v,h,m) \\ \text{and}\quad \frac{\mathrm{d}^\alpha m}{\mathrm{d}t^\alpha} &= 4[g(a_3,\ b_3+V_{K2}^{\text{shift}},\ v)-m] = f_3(v,h,m), \end{aligned}\right\} \tag{2.1}$$

where v measures the membrane voltage. The state variables h and m represent the membrane channel gating variables where h is considered with the fast ionic channels such as sodium ion channels and m is associated with the slow gating variable. $\alpha \in (0,\ 1]$ is the fractional exponent. A Boltzmann function, $g(a_i,\ b_i,\ v) = 1/(1+\mathrm{e}^{a_i(b_i+v)})$, $\forall i = 1, 2, 3$ (a_i and b_i are constant parameters) is associated with the formulation of the excitable model that describes the kinetics of the activation/inactivation of ionic currents. The simplified model is based on the dynamics of the sodium and potassium currents. V_{K2}^{shift} is the experimentally observable predominant parameter of the classical-order system that has a deviation from the average membrane potential value $v = -0.018$ V corresponding to the semi-activated potassium ion channels when the Boltzmann function $g = 1/2$ [47–49]. The model in fractional domain has rich varieties of spiking and bursting behaviour which will be described (in detail) in §4.

3. Preliminaries, stability analysis and numerical method

To study the FOD of the L-H model, we introduce the familiar definition of the fractional derivative i.e. the Caputo-order fractional derivative [8–10]. The commensurate fractional-order system can be described as

$${}^cD_{0,t}^\alpha z(t) = f(z(t)), \tag{3.1}$$

with initial condition $z(0) = (z_1(0),\ z_2(0), \ldots z_n(0))^{\mathrm{T}}$, where $z(t) \in \mathbb{R}^n, {}^cD_{0,t}^\alpha z(t) = ({}^cD_{0,t}^\alpha z_1(t),\ {}^cD_{0,t}^\alpha z_2(t),\ \ldots, {}^cD_{0,t}^\alpha z_n(t))^{\mathrm{T}} \in \mathbb{R}^n$, the fractional-order lies in $0 < \alpha < 1$ and $f(z(t)) = (f_1(z(t)),\ f_2(z(t)),\ \ldots,\ f_n(z(t)))^{\mathrm{T}} \in \mathbb{R}^n$. Suppose the fixed point of the system (3.1) is $z^* = (z_1^*,\ z_2^*,\ \ldots,\ z_n^*)^{\mathrm{T}}$. For the asymptotic stability of the fixed point z^*, we consider a small perturbation $\eta(t)$ from the fixed point z^*, i.e. $z(t) = \eta(t) + z^*$,

Downloaded from https://royalsocietypublishing.org/ on 23 May 2022

where $\eta(t) = (\eta_1(t),\ \eta_2(t), \ldots,\ \eta_n(t))^{\mathrm{T}}$. The system (3.1) can be rewritten as

$$\begin{aligned} {}^{c}D^{\alpha}_{0,t} z(t) &= {}^{c}D^{\alpha}_{0,t}(\eta(t) + z^*) \\ &= f_i(\eta_1(t) + z_1^*,\ \eta_2(t) + z_2^*,\ \ldots,\ \eta_n(t) + z_n^*,), \\ i &= 1, 2, \ldots, n. \end{aligned} \tag{3.2}$$

Since we know that ${}^{c}D^{\alpha}_{0,t} z^*(t) = 0$, we have

$$\begin{aligned} {}^{c}D^{\alpha}_{0,t}\eta(t) &= f_i(\eta_1(t) + z_1^*,\ \eta_2(t) + z_2^*,\ \ldots,\ \eta_n(t) + z_n^*), \\ i &= 1, 2, \ldots, n. \end{aligned} \tag{3.3}$$

The Taylor series expansion of the right side of system (3.3) is as follows:

$$\begin{aligned} f_i(\eta_1(t) + z_1^*,\ \eta_2(t) + z_2^*,\ \ldots,\ \eta_n(t) + z_n^*) &= f_i(z_1^*,\ z_2^*,\ \ldots,\ z_n^*) \\ + \left[\left.\frac{\partial f_i}{\partial z_1}\right|_{z^*} \cdots \left.\frac{\partial f_i}{\partial z_n}\right|_{z^*}\right]\eta(t) &+ \text{h.o.t.}, \end{aligned} \tag{3.4}$$

where $\eta(t) = [\eta_1(t),\ \eta_2(t), \ldots,\ \eta_n(t)]^{\mathrm{T}}$. We know that $f_i(z_1^*, z_2^*, \ldots, z_n^*) = 0$ for $i = 1, 2, \ldots, n$, therefore:

$$\begin{aligned} f_i(\eta_1(t) + z_1^*,\ \eta_2(t) + z_2^*,\ \ldots,\ \eta_n(t) + z_n^*) \\ \approx \left[\left.\frac{\partial f_i}{\partial z_1}\right|_{z^*} \left.\frac{\partial f_i}{\partial z_2}\right|_{z^*} \cdots \left.\frac{\partial f_i}{\partial z_n}\right|_{z^*}\right]\eta(t). \end{aligned}$$

The linearized fractional-order system can be written as

$${}^{c}D^{\alpha}_{0,t}\eta(t) = J|_{z^*}\eta(t), \tag{3.5}$$

with initial condition $\eta(0) = (\eta_1(0), \eta_2(0), \ldots, \eta_n(0))^{\mathrm{T}}$ where $J = \partial f_i/\partial z_i|_{z^*}$ for $i = 1, 2, \ldots, n$. The variable z is considered as $z \equiv (v,\ h,\ m)^{\mathrm{T}}$. The jacobian matrix ($J$) is described in appendix A.

Remark 3.1. The stability of the fixed point (z^*) of the fractional-order system (3.1) can be explained by the stability of the linearized system (3.5) at the same fixed point (z^*) i.e. the fixed point of the nonlinear system (3.1) is asymptotically stable if the fixed point of linearized system (3.5) is asymptotically stable [51,52].

Definition 3.2. [53,54] The equilibrium point (system (3.5)) is locally asymptotically stable iff all the eigenvalues of the Jacobian matrix of the linearized system evaluated at the equilibrium solution satisfies the condition $|\arg(eig(J|_{z^*}))| > \pi\alpha/2$. In a three-dimensional nonlinear dynamical system, an equilibrium point which is a saddle point, is called a saddle of index one if corresponding to this equilibrium point one of the eigenvalues is unstable and the other two eigenvalues are stable. Then, a saddle point of index two represents a saddle point with one stable eigenvalue and two unstable eigenvalues [54]. Moreover, it was observed that scrolls are produced only around the saddle points of index two and saddle points of index one are responsible for connecting the scroll attractors in chaotic dynamical systems [54].

Definition 3.3. [54,55] A necessary condition for a nonlinear fractional-order system to remain chaotic is keeping the eigenvalue λ in the unstable region. It shows that $\alpha > (2/\pi)\tan^{-1}(|\mathrm{Im}(\lambda)|/\mathrm{Re}(\lambda))$.

Suppose the system (3.1) becomes an incommensurate fractional-order system, then the stability condition for the equilibrium point is given by the following definition.

Definition 3.4. [56] Suppose the fractional orders are considered as $0 < \alpha_i = x_i/y_i < 1$, such that $g.c.d\ (x_i, y_i) = 1$ for $i = 1, 2, \ldots, n$, then the equilibrium point of the incommensurate model is asymptotically stable if all the roots ξ of the characteristic equation $\det(\mathrm{diag}(\xi^{L\alpha_1}, \xi^{L\alpha_2}, \ldots, \xi^{L\alpha_n}) - J|_{z^*}) = 0$ satisfy $|\arg(\xi)| > \pi/2L$, where L is the l.c.m of y_i's of α_i's.

3.1. Numerical scheme

We consider the fractional-order derivative (in Caputo sense) of a variable $z \equiv (v,\ h,\ m)^{\mathrm{T}}$ as follows:

$$D^{\alpha} z = f(z,\ t), \tag{3.6}$$

where, $\alpha \in (0,\ 1)$ and $f \equiv (f_1,\ f_2,\ f_3)^{\mathrm{T}}$. Using the definition, we obtain

$$D^{\alpha}\begin{bmatrix} v(t) \\ h(t) \\ m(t) \end{bmatrix} = \frac{1}{\Gamma(1-\alpha)}\int_0^t (t-\tau)^{-\alpha}\begin{bmatrix} v'(\tau) \\ h'(\tau) \\ m'(\tau) \end{bmatrix} \mathrm{d}\tau, \tag{3.7}$$

where the gamma function is described as $\Gamma(x) = \int_0^{\infty} \mathrm{e}^{-t} t^{x-1}\,\mathrm{d}t$.

The Caputo-order derivative is consistant with the physical initial and boundary conditions. In this case, the firing characteristics of the system are strongly independent of the initial conditions [8,20]. An additional advantage in this case is that the derivative of a constant is zero. We can also define, the initial conditions for the fractional-order system that can be handled using an analogy with the classical-order derivative. It includes a memory effect with a convolution between the classical-order derivative and a power of time. It is efficient to integrate all the previous activities of the function weighted by a function that follows power law dynamics. Now, applying the L1 scheme [8,13,16,17,25] on the system (3.7) and approximate the fractional-order derivative as follows:

$$\begin{aligned} D^{\alpha}\begin{bmatrix} v(t) \\ h(t) \\ m(t) \end{bmatrix} &= \frac{(\mathrm{d}t)^{-\alpha}}{\Gamma(2-\alpha)} \\ \begin{bmatrix} \sum_{k=0}^{N-1} [v(t_{k+1}) - v(t_k)][(N-k)^{1-\alpha} - (N-1-k)^{1-\alpha}] \\ \sum_{k=0}^{N-1} [h(t_{k+1}) - h(t_k)][(N-k)^{1-\alpha} - (N-1-k)^{1-\alpha}] \\ \sum_{k=0}^{N-1} [m(t_{k+1}) - m(t_k)][(N-k)^{1-\alpha} - (N-1-k)^{1-\alpha}] \end{bmatrix}. \end{aligned} \tag{3.8}$$

The numerical solution of (3.6) can be formulated as (combining (3.6) and (3.8))

$$\begin{aligned} v(t_N) \approx (\mathrm{d}t)^{\alpha}\Gamma(2-\alpha) f_1(v(t), h(t), m(t)) + v(t_{N-1}) \\ - \left[\sum_{k=0}^{N-2} [v(t_{k+1}) - v(t_k)][(N-k)^{(1-\alpha)} - (N-1-k)^{(1-\alpha)}]\right], \end{aligned}$$

where, t_k represents the kth time step and $t_k = k\Delta t$. Similarly, we can derive the other two expressions. Hence, the numerical solution of (3.6) can be summarized as the difference between the Markov term weighted by the gamma function

Downloaded from https://royalsocietypublishing.org/ on 23 May 2022

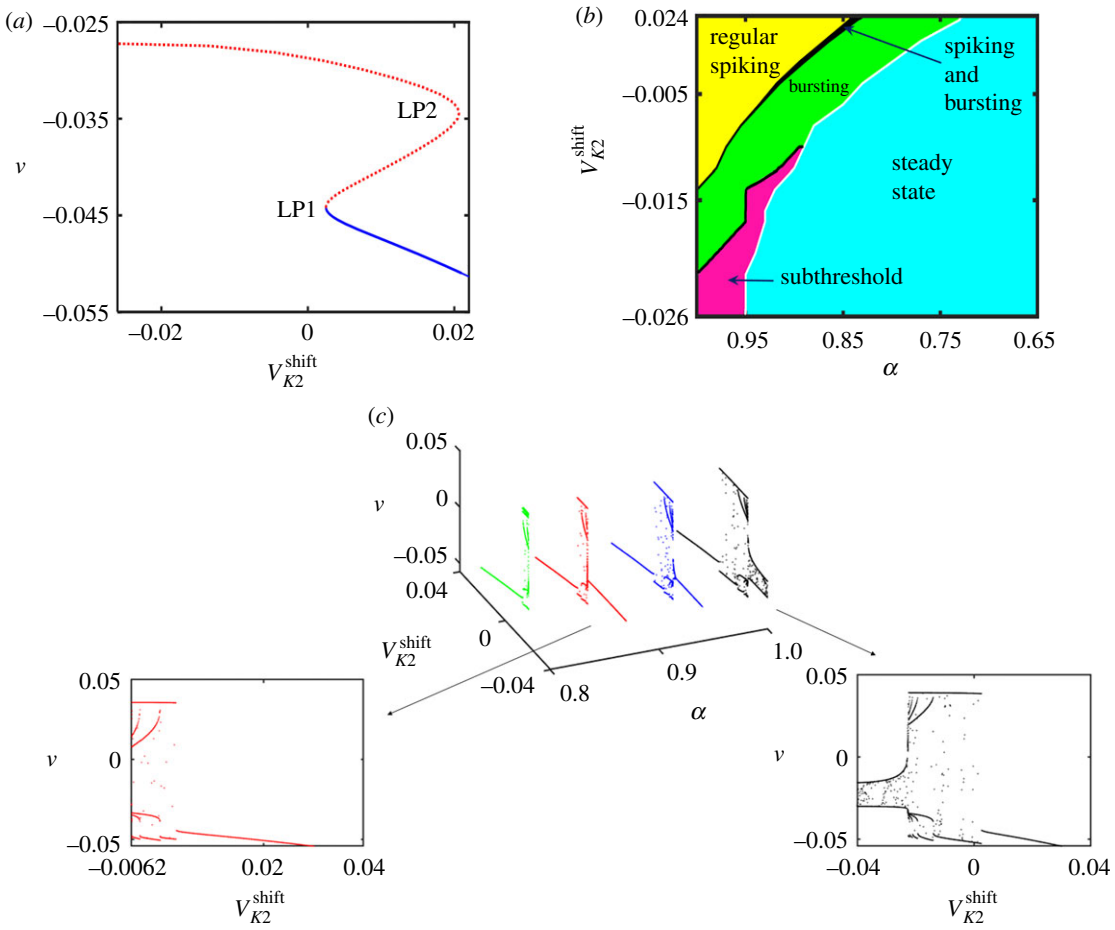

Figure 1. Bifurcation diagram of classical-order uncoupled L-H model and two-parameters bifurcation analysis in the presence of FOD. (*a*) V_{K2}^{shift} is considered as the predominant parameter. *LP*1 and *LP*2 denote the saddle-node bifurcation points, whereas the thick blue and dotted red lines indicate the stable and unstable equilibrium states respectively. (*b*) Parameter-space analysis: the various firing activities that depends on the parameter V_{K2}^{shift} with different fractional-orders α. (*c*) A 3D representation of bifurcation diagram: green, red, blue and black slices represent the dynamics of the system (2.1) at fractional orders 0.82, 0.87, 0.95 and 1, respectively. For better visualization, we have shown the two slices for different α.

and the memory trace. Memory trace has the main functional role in the fractional-order system as it integrates all the past activities. The memory trace has no effect for $\alpha = 1$. The non-linearity in the memory trace increases as we decrease the fractional-order α from 1 and the system dynamics depends on time. The commensurate fractional-order L-H system is numerically integrated using this scheme. The Markov term weighted by the gamma function is given by $(\mathrm{d}t)^{\alpha}\Gamma(2-\alpha)f(z,\ t) + z(t_{N-1})$ and the memory trace (v, h, m-memory) is given by

$$\left[\sum_{k=0}^{N-2}[z(t_{k+1}) - z(t_k)][(N-k)^{(1-\alpha)} - (N-1-k)^{(1-\alpha)}]\right].$$

4. Analytical results and different dynamical responses of the fractional-order leech-heart model

We analyse the fractional-order system in three different regimes: bursting, regular spiking and phasic spiking, respectively. We have considered four different parameter sets from the above-mentioned regimes as follows [47] $a_1 = -150$, $b_1 = 0.0305$, $a_2 = 500$, $b_2 = 0.0333$, $a_3 = -83$, $b_3 = 0.018$, set I: $V_{K2}^{shift} = -0.021$, set II: $V_{K2}^{shift} = -0.015$, set III: $V_{K2}^{shift} = 0.001$ and set IV: $V_{K2}^{shift} = 0.003$, respectively.

Bifurcation analysis. Bifurcation analysis plays an important role in analysing and determining the different qualitative properties of any dynamical system. We performed the bifurcation analysis of the classical-order model using the MATCONT software [57]. V_{K2}^{shift} is considered as the predominant parameter while other parameters are at their base values. The steady state disappears through a saddle-node bifurcation at $V_{K2}^{shift} = 0.002471$ (LP1), where one stable and one unstable equilibrium points collide and mutually annihilate. Again there is a saddle-node bifurcation at $V_{K2}^{shift} = 0.020652$ (LP2). The thick blue and dotted red lines indicate the stable and unstable equilibrium states, respectively (figure 1*a*). The system has a stable focus node for $0.0025 < V_{K2}^{shift} < 0.012$ and a stable node for $V_{K2}^{shift} > 0.012$, respectively. The system has an unstable focus node for $V_{K2}^{shift} < 0.0024$. The classical-order L-H model shows periodic bursting for $-0.024 < V_{K2}^{shift} \leq -0.015$ (figure 1*b*, extreme left green regime). As we decrease the value of V_{K2}^{shift} from −0.01 to −0.025, the classical order system goes through a series of period-adding bifurcation and chaotic state exists around the parameter value −0.024 [49]. This region shows limit cycle and chaotic attractor. A chaotic window exists in the neighbourhood of $V_{K2}^{shift} = -0.021$, that belongs to this attractor state [47]. As we increase the value of V_{K2}^{shift}

Downloaded from https://royalsocietypublishing.org/ on 23 May 2022

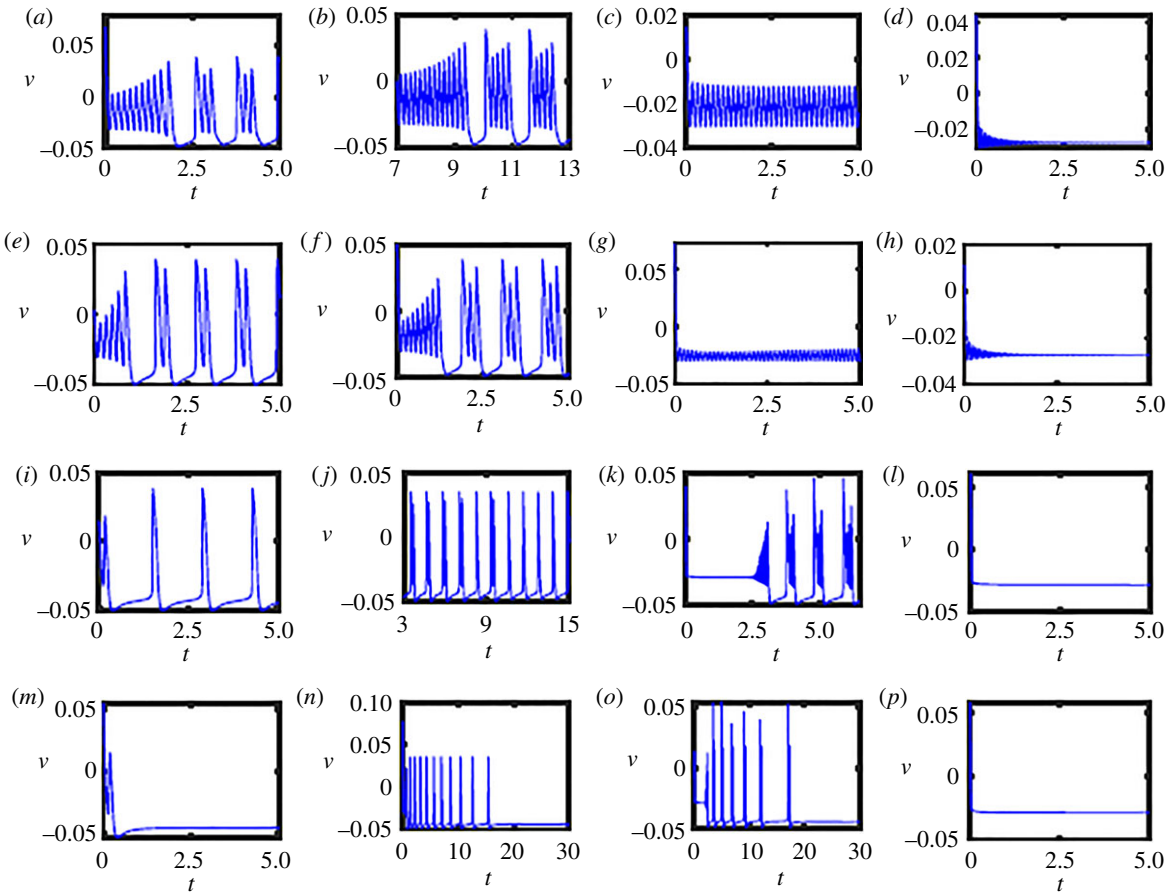

Figure 2. Time series of uncoupled fractional-order L-H model for different fractional exponents. Set I: $V_{K2}^{\text{shift}} = -0.021$ (*a*)–(*d*) $\alpha = 1, 0.99, 0.98, 0.94$. Set II: $V_{K2}^{\text{shift}} = -0.015$ (*e*)–(*h*) $\alpha = 1, 0.97, 0.94, 0.92$. Set III: $V_{K2}^{\text{shift}} = 0.001$ (*i*)–(*l*) $\alpha = 1, 0.85, 0.78, 0.72$. Set IV: $V_{K2}^{\text{shift}} = 0.003$ (*m*–*p*) $\alpha = 1, 0.83, 0.75, 0.68$.

($-0.014 < V_{K2}^{\text{shift}} \leq 0.0025$), it exhibits spiking (figure 1*b*, extreme left yellow regime). Further, with the increase of V_{K2}^{shift}, the system shows phasic spiking and later it converges to steady state. The firing patterns produced from the voltage memory trace are almost similar to membrane voltage. Further with the decrease of the fractional exponent (α), it leads to the system in steady state i.e. memory traces become too weak to generate an action potential i.e. spike. The fractional-order L-H model shows different types of firing patterns controlled by the fractional-order α and predominant parameter V_{K2}^{shift} (figure 1*b*). Steady state and subthreshold regimes are shown by cyan and magenta colour, respectively, whereas green, black and yellow regimes indicate that the fractional-order system is in different oscillatory modes (bursting, spiking–bursting and tonic spiking) (figure 1*b*). The white line in the figure 1*b*, that separates the oscillatory regime from steady state is derived through analytical treatment based on stability analysis of FOD. A 3D representation of the bifurcation analysis for various α is shown in the figure 1*c*. Green, red, blue and black slices represent the dynamics of the system (2.1) at $\alpha = 0.82, 0.87, 0.94$ and 1, respectively. We observed from figure 1*c*, how the fractional order plays an important role in stabilizing the complex system. For various V_{K2}^{shift}, the system goes through different transition states of oscillations as we vary α. We explore this parameter space from excitable to oscillatory regime for diverse fractional orders [47].

Example 4.1. First, we consider the parameter set I ($V_{K2}^{\text{shift}} = -0.021$), where the classical-order model shows bursting with three spikes per burst after some transient portion. The equilibrium point at the parameter set I is $E_1 = (v^*, h^*, m^*) = (-0.0272187, 0.0456, 0.0753)$. The eigenvalues of the Jacobian matrix at E_1 are $\lambda_{1,2} = 4.22743 \pm 53.7296i$ and $\lambda_3 = -4.06256$. Using definition 3.1, we obtained that E_1 is asymptotically stable for $\alpha < 0.950014$. E_1 is a saddle point of index two for classical-order system. We obtained the Lyapunov exponents (LEs) $=(0.001736, -3.744327, -39.210317)$ using Wolf algorithm and Runge–Kutta fourth order method with time step 0.01 [58]. The positive LE indicates the system exhibits chaos in the neighbourhood of $V_{K2}^{\text{shift}} = -0.021$ for $\alpha = 1$. Moreover, the fractional-order system exhibits chaotic behaviour for $\alpha > 0.950014$, which is in good agreement with the numerical simulation. With $\alpha = 0.99$, the system shows regular bursting, however the number of spikes per burst increases and it has a longer transient part i.e. a first spike latency. When we decrease $\alpha = 0.98$, it produces subthreshold oscillations and the membrane voltage dynamics converges to quiescent state when α converges to 0.94 (figure 2*a*–*d*).

Example 4.2. As we increase the value of the predominant parameter $V_{K2}^{\text{shift}} = -0.015$ (set II) the behaviour of the classical-order model remains same as mentioned above, however, the number of spikes per burst decreases i.e. there are two spikes per burst after some transient period and interspike interval decreases i.e. firing frequency increases. The eigenvalues of the Jacobian matrix at the fixed point $E_2 = (v^*, h^*, m^*) = (-0.027389, 0.0495, 0.1167)$ are $\lambda_{1,2} = 5.85805 \pm 54.7294i$ and $\lambda_3 = -4.13658$. E_2 is asymptotically stable for $\alpha < 0.932117$. Here, E_2 is a saddle point of index two for classical-order

Downloaded from https://royalsocietypublishing.org/ on 23 May 2022

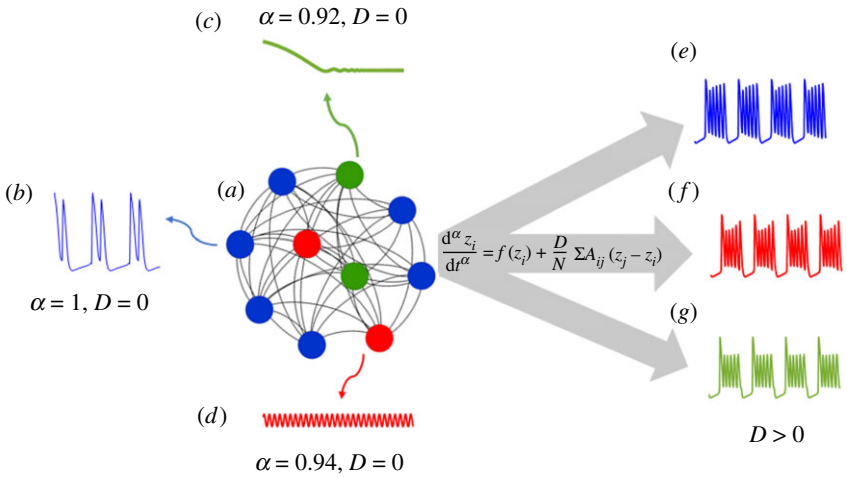

Figure 3. Schematic diagram of firing activities of fractional and classical L-H neurons in presence (absence) of coupling (D) for parameter set II, see §§2 and 4 for model description and parameter specification. (*a*) A network of 10 nodes. Six blue nodes exhibit bursting shown in (*b*) for classical L-H neurons in the absence of fractional exponent (α). In the presence of FOD (*c*) two green nodes are in quiescent states and (*d*) two red nodes reveal subthreshold oscillations. (*e–g*) After coupling is introduced, entire network periodically fires (bursts) together.

system. With $\alpha = 0.97$, the fractional-order excitable system generates periodic bursting, and the number of spikes per burst increases. When we decrease α to 0.94, it produces subthreshold oscillations and the membrane voltage dynamics dies out when α converges to 0.92 (figure 2*e–h*).

Example 4.3. Now, we consider the parameter set III ($V_{K2}^{\text{shift}} = 0.001$) where the classical-order model exhibits single periodic spiking. The eigenvalues of the Jacobian matrix at the fixed point $E_3 = (v^*,\ h^*,\ m^*) = (-0.0288274,\ 0.0965,\ 0.3067)$ are $\lambda_{1,2} = 23.5907 \pm 58.9194i$ and $\lambda_3 = -4.52285$. E_3 is asymptotically stable for $\alpha < 0.757548$. E_3 is a saddle point of index two. With the decrease of α to 0.85, the system generates mixed-mode type oscillations, first bursting then single spiking. When we decrease α to 0.78, it has a transition to bursting with spike latency. The system goes to quiescent state when the fractional exponent converges to $\alpha = 0.72$ (figure 2*i–l*).

Example 4.4. Finally, we consider the phasic spiking regime i.e. set IV ($V_{K2}^{\text{shift}} = 0.003$), where the classical-order model fires only a single spike at the onset of the input stimulus current and remain quiescent afterwards (figure 2*m*). The eigenvalues of the Jacobian matrix at the fixed point $E_4 = (v^*,\ h^*,\ m^*) = (-0.0291305,\ 0.1106,\ 0.3374)$ are $\lambda_{1,2} = 28.2715 \pm 58.271i$ and $\lambda_3 = -4.57275$. E_4 is asymptotically stable for $\alpha < 0.712429$. E_4 is a saddle point of index two. As we decrease the fractional-order to $\alpha = 0.83$, the system shows regular spiking with spike frequency adaptation and it converges to steady state after some time elapsed. With $\alpha = 0.75$, the excitable system exhibits bursting. However, the train of spikes converges to the oscillation death condition after some time duration though the current stimulus is applied. When we further decrease $\alpha = 0.68$, the fractional-order system converges to complete quiescent state (figure 2*m-p*). The numerical integration scheme of the FOD is described in §3.1.

In the next section, we will explore our main results: how the mixed population of fractional-order single L-H neurons with different characteristic behaves under diffusive coupling over a broad range of coupling strength (D).

5. Network of L-H neurons

To illustrate the network dynamics, we consider a small network having global coupling topology (figure 3*a*). This network (in the absence of synaptic coupling strength D) consists of three types of neuronal oscillations (based on FOD): six blue nodes have periodic bursting (figure 3*b*) in which α is unity (classical integer order system). Two green nodes are in quiescent states (figure 3*c*, $\alpha = 0.92$) and two red nodes show subthreshold oscillations (figure 3*d*, $\alpha = 0.94$). Note that these oscillatory and steady-state behaviours are drastically different to each other due to the significant changes of memory properties in fractional domain (α). We use them as nodal dynamics over the top of a globally coupled network. After the coupling (D) is introduced, the network fires together with regular bursting having multiple spikes (figure 3*e–g*) for a certain range of coupling strengths. This is an interesting and unique behaviour which cannot be identified in a single unit of fractional node. Now, we have considered N number of mixed fractional L-H neuron models in which a single neuron reveals diverse recurrent spiking features or quiescent characteristics. We also assume that the L-H neurons are diffusively [59] connected (electrical coupling) through voltage variable. The network of oscillators can be captured by

$$\frac{\mathrm{d}^{\alpha_i}\mathbf{z_i}}{\mathrm{d}t^{\alpha_i}} = f(\mathbf{z_i}) + \frac{D}{N}\sum_{j=1}^{N}(\mathbf{z_j} - \mathbf{z_i}), \quad i = 1, 2, \ldots N, \tag{5.1}$$

where D is the coupling strength, and the considered flow vector follows the L-H interneuron model. Therefore, $\mathbf{z_i}(t) = [v_i(t),\ h_i(t),\ m_i(t)]^{\mathrm{T}}$ and $f : \mathbb{R}^3 \to \mathbb{R}^3$. The sets of fractional parameters are introduced as follows:

$$\alpha_i\boldsymbol{\alpha} = [\underbrace{\alpha, \ldots, \alpha}_{p}, \underbrace{\beta, \ldots, \beta}_{q}, \underbrace{\gamma, \ldots, \gamma}_{r}, \underbrace{\delta, \ldots, \delta}_{s}], \tag{5.2}$$

in which p number of nodes will have identical fractional exponent α, the rest q, r and s nodes have β, γ and δ exponents, respectively. If the total population size is N, we can write

$$p + q + r + s = N. \tag{5.3}$$

In this article, we have considered two and three types of mixed population depending on the FOD. Generally, the

Downloaded from https://royalsocietypublishing.org/ on 23 May 2022

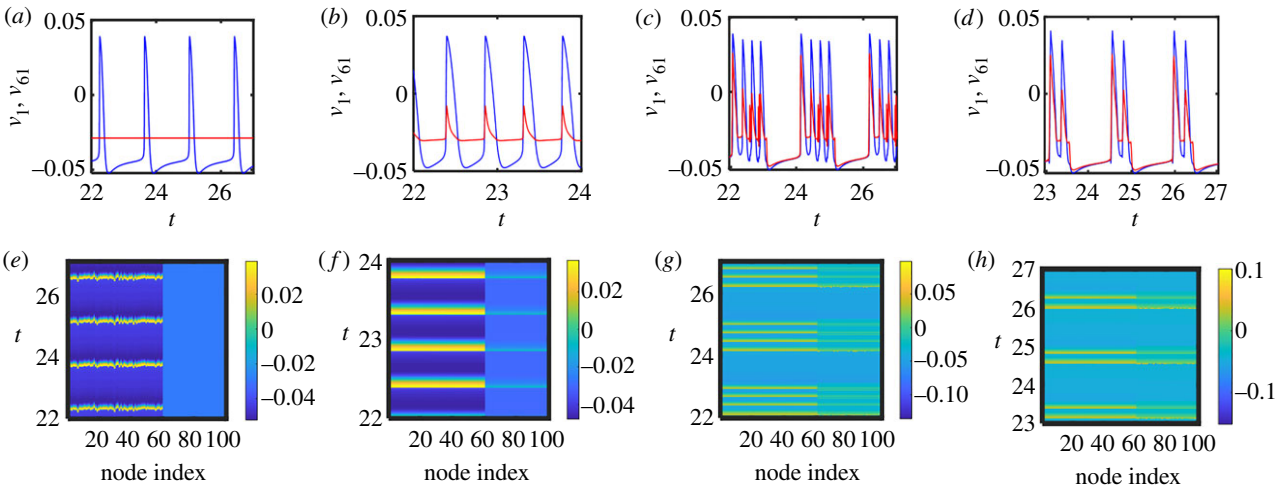

Figure 4. Time evaluation and spatio-temporal dynamics of nodes in coupled networks having two types of fractional exponents. Time series of oscillatory nodes (v_1) and excitable nodes (v_{61}) and the temporal dynamics of all the nodes for fractional-orders $\alpha_1 = \alpha_2 = \cdots = \alpha_{60} = 1$ and $\alpha_{61} = \alpha_{62} \cdots = \alpha_{100} = 0.65$ at $V_{K2}^{\text{shift}} = 0.001$ (set III) for various coupling strengths: (*a*,*e*) $D = 0$, (*b*,*f*) $D = 20$, (*c*,*g*) $D = 40$ and (*d*,*h*) $D = 47$ are shown.

uncoupled neuron has three types of neuronal responses: bursting (parameter sets I–II), spiking (parameter set III) and phasic spiking (parameter set IV). The neurocomputational features can be reproduced by varying the fractional exponents in the single neuron model for a certain parameter space. Therefore, we connect a mixed network of N neurons in which maximum three different types of neuronal activities (where at least one fraction of populations will be in quiescent or steady state at $D = 0$) will act together. In this backdrop, our motivation is to generate bursting in the entire network. For simplicity, first, we consider two subpopulations of L-H neurons in which p number of fractional L-H nodes are in oscillatory mode and q neurons are in excitable mode ($p + q = N$). A network of 100 neurons ($N = 100$) is considered for numerical simulations.

We begin our analysis by considering the parameter set III, where the classical-order model ($p = 60$) shows a train of single spikes (figure 4*a* in blue colour) ($\alpha_{1,\ldots,60} = \alpha = 1$). The classical-order model is coupled with a subpopulation ($q = 40$) of memory-dependent excitable oscillations ($\alpha_{61,\ldots,100} = \beta = 0.65$, (figure 4*a* in red colour)) via the membrane voltage v_i. The oscillatory subpopulation is de-synchronized within subpopulation and across the subpopulation when there is no coupling i.e. $D = 0$. As we increase the coupling to $D = 20$, an interesting feature is observed: the quiescent oscillators started to show subthreshold oscillations and the quiescence period of the regular spiking decreases (figure 4*b*). Here, the two subpopulations are separately clustered and completely synchronized within their own domain (figure 4*f*). At higher electrical coupling ($D = 40$), the entire population bursts almost together with multiple spikes (four) per burst (figure 4*c*), a unique feature that can never be produced in the uncoupled L-H neurons. Further increase of D ($D = 45$) reduces the spikes (3) per burst and at $D = 47$, it shows two spikes per burst (figure 4*d*). Interestingly, the oscillatory subpopulation was de-synchronized at lower coupling, whereas two cluster states (synchronization within subpopulation) pop up at higher coupling and more we increase the strength the bursts follow in phase relation across the entire network (see the spatio-temporal dynamics in figure 4*f* –*h*). In the next subsection, we will use these synchronization dynamics to reduce the entire network into fewer equations depending on the number of synchronous clusters. Note that, the slow dynamics is essential for the generation of bursting dynamics in the network and it is provided by the excitable neurons [60]. Thus, the presence of small groups of excitable units create bursting in the network even though the uncoupled system never exhibits bursting dynamics.

Now, we extend our study by considering the network as a composition of three different subpopulations and observed the effects of coupling for different parameter sets. The size of these three subpopulations are considered as $p = 60$, $q = 20$ and $r = 20$ ($p + q + r = N = 100$) neurons respectively. At parameter set III, we consider the system where it generates regular spiking ($\alpha_{1,\ldots,60} = \alpha = 1$), bursting ($\alpha_{61,\ldots,80} = \beta = 0.78$) and quiescent state ($\alpha_{81,\ldots,100} = \gamma = 0.65$) (figure 5*a*). In the absence of coupling, all the neurons within the cluster are de-synchronized (figure 5*d*) but as we increase the value of coupling strength, the entire population shows bursting (figure 5*b*,*c*) and all three subpopulations exhibit complete synchronization within the cluster (figure 5*e*,*f*). Note that the bursting activities of coupled fractional and classical L-H neurons (three mixed population) shown in the schematic diagram (figure 3) have been explored for the parameter set II. The coupling has been considered at $D = 30$.

Next, we consider the system at parameter set IV (three subpopulations with same size as described above) where it shows phasic spiking ($\alpha = 1$, blue line in figure 5*g*), spiking for a short time and then converges to a quiescent state ($\beta = 0.83$, red line in figure 5*g*) and oscillation death ($\gamma = 0.68$, black line in figure 5*g*). Now, we increase the value of coupling to $D = 5$, the oscillators that were in phasic spiking mode or the oscillators frequency adapting steady states start to oscillate periodically (figure 5*h*,*k*). Even the oscillators having oscillation death ($\gamma = 0.68$) states (in absence of coupling) are showing low amplitude regular oscillations for a long-term evaluation. The complete set of neurons which were silent in uncoupled states are firing collectively, a counterintuitive phenomena cannot be captured without coupling and without parameter heterogeneity. As described above, these three clusters are separately synchronized within itself and in the next section,

Downloaded from https://royalsocietypublishing.org/ on 23 May 2022

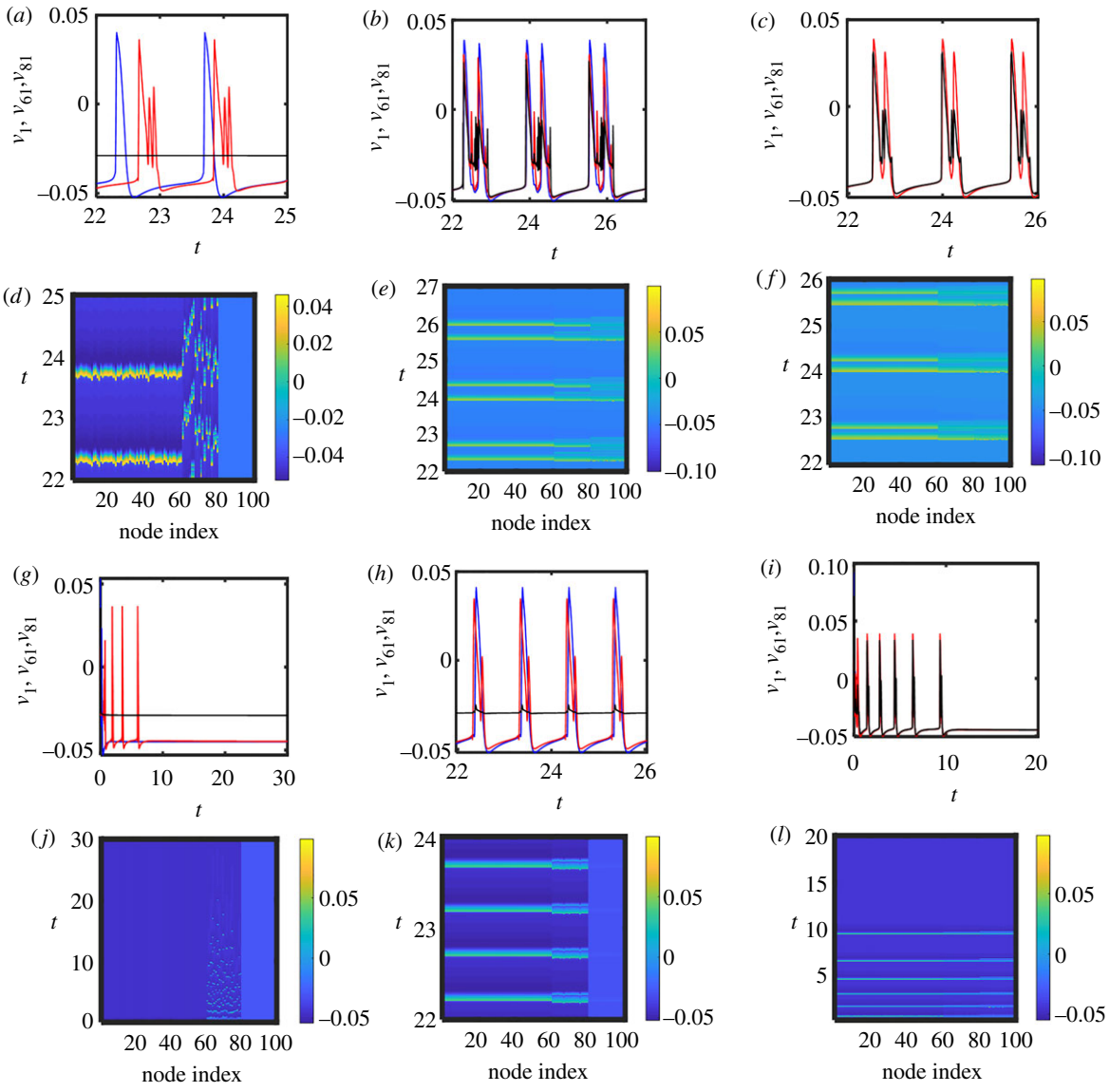

Figure 5. Time evaluation and spatio-temporal dynamics of nodes in coupled networks having three types of fractional exponents. Time series of three nodes, one represents all the oscillatory nodes (v_1) and other represents all the excitable nodes (v_{61} and v_{81}) and the temporal dynamics of all the nodes for various coupling strengths and fractional-orders are shown: (*a*,*d*) $D = 0$, (*b*,*e*) $D = 25$, (*c*,*f*) $D = 35$ and $\alpha_1 = \alpha_2 = \cdots = \alpha_{60} = 1$, $\alpha_{61} = \alpha_{62} \cdots = \alpha_{80} = 0.78$, $\alpha_{81} = \alpha_{82} \cdots = \alpha_{100} = 0.65$ at $V_{K2}^{\text{shift}} = 0.001$ (set III). (*g*,*j*) $D = 0$, (*h*,*k*) $D = 5$, (*i*,*l*) $D = 28$ and $\alpha_1 = \alpha_2 = \cdots = \alpha_{60} = 1$, $\alpha_{61} = \alpha_{62} \cdots = \alpha_{80} = 0.83$, $\alpha_{81} = \alpha_{82} \cdots = \alpha_{100} = 0.68$ at $V_{K2}^{\text{shift}} = 0.003$ (set IV).

we will design a reduced-order model description to reflect the nature and states of entire network. At higher coupling, the network converges to quiescent state after showing bursting with adaptation up to a limited small time span ($D = 28$) (figure 5*i*,*l*). With significantly more higher coupling we expect the coupled neurons will return to excitable states together. This is closely analogous to the emergence of Turing-like pattern in coupled neurons [61] in which inhomogeneity occurs at intermediate diffusion and homogeneity re-emerge for higher diffusion.

5.1. Reduced-order model description

We seek a general and low-dimensional model description which can perform same feature as observed in large networks. To proceed further, we carefully examine the spatio-temporal plot for higher coupling strength in which the nodes having identical exponent fire synchronously. Based on this spatio-temporal dynamics, we can provide a general proposition to reconstruct a reduced-order model [60,62,63].

Proposition 5.1. If we have a network of N nodes and n ($n < N$) number of synchronized clusters (favourably for different size) then we can reduce the network in n number of oscillators for considerably higher diffusive coupling strength.

Assume three ($n = 3$) types of exponents (α, β and γ) exist for the population of size N, and the size of each subpopulation p, q and r, respectively. In cluster synchronization domain, we may write

$$\underbrace{\mathbf{z_1} = \cdots = \mathbf{z_p}}_{p} = \mathbf{Z_\alpha};\ \underbrace{\mathbf{z_{p+1}} = \cdots = \mathbf{z_{p+q}}}_{q} = \mathbf{Z_\beta};\ \underbrace{\mathbf{z_{p+1+q}} = \cdots = \mathbf{z_{p+q+r}}}_{r} = \mathbf{Z_\gamma}. \tag{5.4}$$

Downloaded from https://royalsocietypublishing.org/ on 23 May 2022

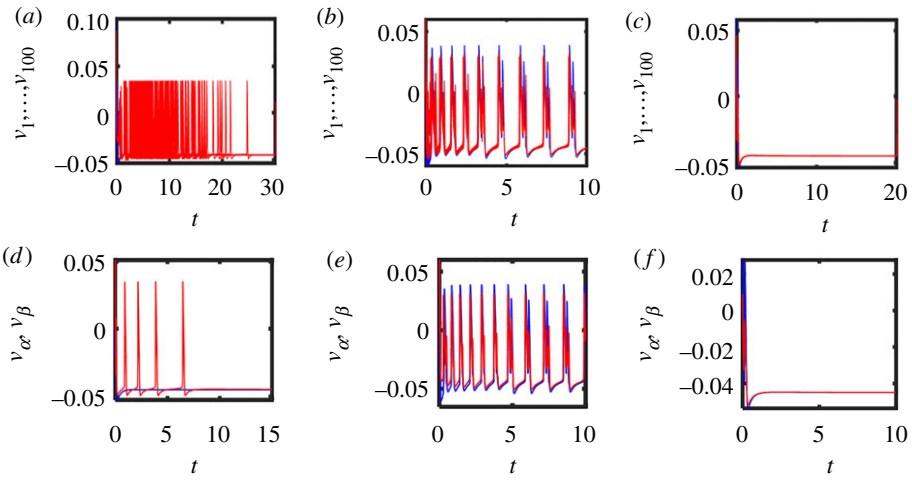

Figure 6. Time evaluation of different nodes in coupled full (*a–c*) and reduced-order model (*d–f*) having two types of fractional exponents $\alpha = 1$ and $\beta = 0.83$ with $p = 0.4$ for various coupling strengths: (*a*,*d*) $D = 0$, (*b*,*e*) $D = 20$ and (*c*,*f*) $D = 40$, respectively (set IV).

Therefore, the entire network can be recast with only three coupled oscillators.

$$\left.\begin{aligned} \frac{\mathrm{d}^\alpha \mathbf{Z}_\alpha}{\mathrm{d}t^\alpha} &= f(\mathbf{Z}_\alpha) + \frac{D}{N}(q(\mathbf{Z}_\beta - \mathbf{Z}_\alpha) + r(\mathbf{Z}_\gamma - \mathbf{Z}_\alpha)), \\ \frac{\mathrm{d}^\beta \mathbf{Z}_\beta}{\mathrm{d}t^\beta} &= f(\mathbf{Z}_\beta) + \frac{D}{N}(p(\mathbf{Z}_\alpha - \mathbf{Z}_\beta) + r(\mathbf{Z}_\gamma - \mathbf{Z}_\beta)) \\ \text{and} \quad \frac{\mathrm{d}^\gamma \mathbf{Z}_\gamma}{\mathrm{d}t^\gamma} &= f(\mathbf{Z}_\gamma) + \frac{D}{N}(p(\mathbf{Z}_\alpha - \mathbf{Z}_\gamma) + q(\mathbf{Z}_\beta - \mathbf{Z}_\gamma)). \end{aligned}\right\} \tag{5.5}$$

If we have a mixed population with two exponents (α and β and $p + q = N$), then the two coupled equations can capture the behaviour of the entire graph. In this situation only the first two equations of (5.5) will exist and the *second term in the coupling will vanish. Note that $\mathbf{Z}_{\alpha,\beta,\gamma}(t) = [v_{\alpha,\beta,\gamma}(t), h_{\alpha,\beta,\gamma}(t), m_{\alpha,\beta,\gamma}(t)]^{\mathrm{T}}$ and an electrical coupling through the membrane voltage v is used. The full equations for three exponents are written in appendix B. The stability [58,59] of synchronization or synchronized clusters is not explored here.

5.2. Stability analysis of the reduced-order model for two subpopulations

We consider the parameter set IV ($V_{K2}^{\mathrm{shift}} = 0.003$) for the analytical treatment of the reduced-order model. The incommensurate model is coupled for different fractional-orders $\alpha = 1$ and $\beta = 0.83$ with $p = 0.4$. From the definition 3.4, we have $x_1 = 1$, $y_1 = 1$, $x_2 = 83$, $y_2 = 100$, here g.c.d $(x_1, y_1) =$ g.c.d$(x_2, y_2) = 1$ and $L =$ l.c.m$(y_1, y_2) = 100$. At $D = 20$, the system has three equilibrium points $(v_\alpha^*, h_\alpha^*, m_\alpha^*, v_\beta^*, h_\beta^*, m_\beta^*)$ given by $P_0 = (-0.0448973, 0.997, 0.1209, -0.0448973, 0.997, 0.1209)$, $P_1 = (-0.0434028, 0.9936, 0.1348, -0.0434028, 0.9936, 0.1348)$ and $P_2 = (-0.0291305, 0.1106, 0.3374, -0.0291305, 0.1106, 0.3374)$. Considering the equilibrium point P_0, we obtain

$$\begin{aligned} &\xi^{549} + 42.0015\xi^{466} + 38.0015\xi^{449} + 495.008\xi^{383} + 1500.12\xi^{366} \\ &\quad + 380.248\xi^{349} + 1638.09\xi^{300} + 16056.8\xi^{283} + 13216.7\xi^{266} \\ &\quad + 1243.05\xi^{249} + 52769\xi^{200} + 109207\xi^{183} + 42729.1\xi^{166} \\ &\quad + 350\,872\xi^{100} + 343\,311\xi^{83} + 1\,099\,890 = 0 \end{aligned}$$

from the equation $\det(\mathrm{diag}(\xi^{L\alpha}, \xi^{L\alpha}, \xi^{L\alpha}, \xi^{L\beta}, \xi^{L\beta}, \xi^{L\beta}) - J|_{z^*}) = 0$. The fixed point is asymptotically stable if all the roots of the above equation satisfy the condition $|\arg(\xi)| > \pi/200$. However, we find a pair of roots, $\xi_{1,2} = -1.02507 \pm 0.0053894i$ that does not satisfy the stability condition (see definition 3.4). Therefore, P_0 is unstable. Similarly, we obtain that the other two equilibrium points P_1 and P_2 are unstable. At higher coupling ($D = 40$), we find that the reduced-order model has two unstable equilibrium points and one stable equilibrium point. Numerically, at $D = 0$, all the oscillators show desynchronized oscillations however, for long evaluations each of them converges to a quiescent state (figure 6*a*). The corresponding reduced-order model also exhibits similar behaviour (figure 6*d*). At an intermediate diffusion ($D = 20$), the full and reduced-order models exhibit bursting (figure 6*b*,*e*), which suggests that the system's fixed points are unstable. We have verified this by analytical treatment (described in the first part of §5.2). Furthermore, with the increase of coupling strength $D = 40$, the system first shows oscillations at the onset and later it converges to stable equilibrium point ($v_\alpha^* = -0.0443$, $v_\beta^* = -0.0442266$, figure 6*c*,*f*). The analytical treatment is not restricted for a specific set of parameters, or two types of population. We can also extend it to other sets of parameters with more than two types of population.

To confirm the effectiveness of our proposition, we have used a statistical measure to verify the level of synchronization within a subpopulation, in which the nodes have identical fractional exponent (say α). We calculate the mean distance from a randomly chosen node (say v_1) from all other oscillatory nodes within that subpopulation. For a long-term evaluation of the variable v, the expression will look like

$$\langle d \rangle = \left\langle \sqrt{\sum_{k=2}^{p} \frac{(v_k - v_1)^2}{p}} \right\rangle, \tag{5.6}$$

in which $\langle\ \rangle$ represents the time average and p is the size (number of oscillators having identical exponent α) of that subpopulation having fractional index α. We calculate $\langle d \rangle$ in parameter set III for three coupling regimes. The variation of $\langle d \rangle$ is shown in the figure 7. At $D = 0$, the neurons having exponent α are desynchronized to each other, therefore the mean distance $\langle d \rangle$ has significantly high positive value.

Downloaded from https://royalsocietypublishing.org/ on 23 May 2022

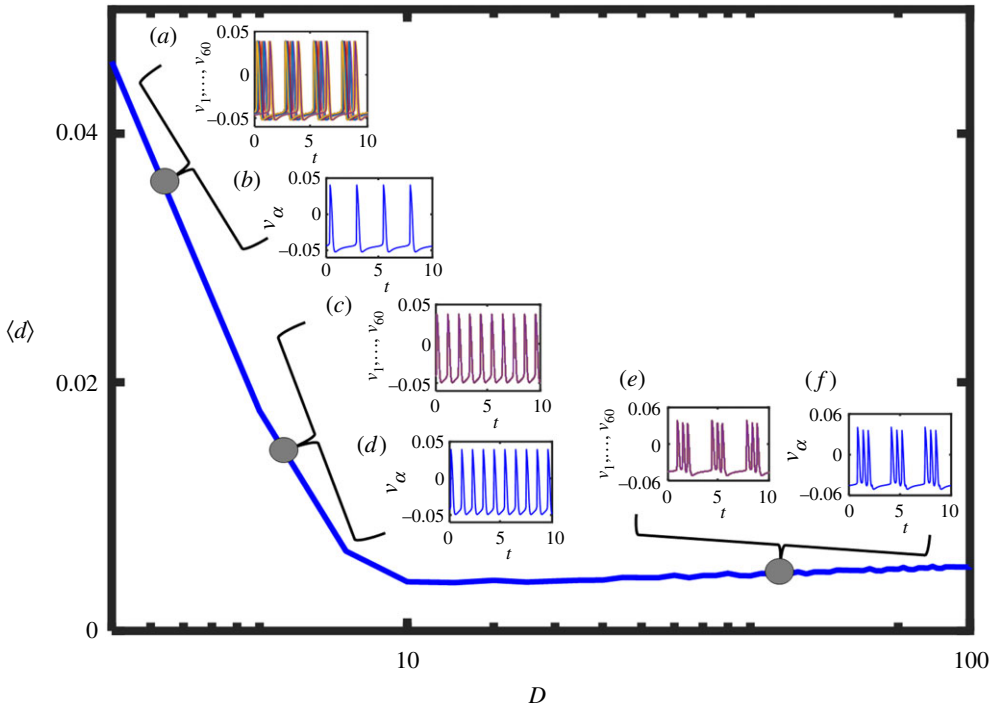

Figure 7. Schematic diagram of average distance of a random node from all other oscillatory nodes at parameter set III for various coupling (D): (*a*) and (*b*) the oscillatory cluster shows desynchronized oscillation at $D = 0$ and the corresponding neuronal response of reduced-order model; (*c*) and (*d*) at low coupling the full model shows synchronized regular spiking and corresponding reduced-order model shows similar behaviour; and (*e*) and (*f*) at higher coupling the full and reduced-order models exhibit periodic bursting.

The desynchronized time evaluation of the entire population ($v_1, \ldots, v_60$) within that subpopulation is shown in figure 7*a*, and the time series of the reduced-order model (v_α) is shown in figure 7*b*. If we introduce the coupling ($D \sim 5$), the population tries to follow coherent motion, therefore $\langle d \rangle$ decreases, which is further confirmed by the bunch of coherent spiking oscillations of all nodes inside the subpopulation (figure 7*c*). As per our proposition, the reduced-order model also show same type of spiking oscillation (figure 7*d*) with fast switching. Periodic bursting emerges at higher coupling ($D \sim 60$) where three spikes in a single burst appear and the mean distance d reduces to zero (figure 7*e*,*f*). The same distance measure ($\langle d \rangle$) can be implemented for the other subpopulation. At considerably higher coupling, each subpopulation will fire in unison (separately) by forming cluster synchronization.

6. Conclusion

The article is mainly based on the study of dynamical behaviour of a fractional-order single and network of L-H interneuron model. In this manuscript, it has been shown how spiking and bursting oscillations generate and converge to steady state through different transition phases in the fractional domain. The fractional-order model can generate various spiking and bursting patterns that can be controlled only using the fractional exponent, α. Bursting emerges with different burst durations and different numbers of spikes appear in one burst. However, the classical-order model cannot reveal such rich varieties of complex dynamics in comparison with it is fractional counterpart. We have also studied the dynamics of the coupled network. A network of $N = 100$ neurons is considered for the numerical simulations. At first, the study has been carried out by taking the network ($N = 100$) into two types of memory settings i.e. dividing them into two subpopulations: 60 spiking neurons whereas another subpopulation consists of 40 excitatory neurons. We have also considered the network as a collection of three subpopulations with three different fractional exponents. Interestingly, for both cases, the entire network fires with burst for a certain coupling strength although the uncoupled neurons cannot reveal bursting at all. We have also uncovered that (at a higher coupling) the network emerges to cluster synchronization where each subpopulation synchronized separately. The formation of cluster synchronization enables us to reduce the network in low-dimensional coupled systems and the results obtained from the reduced-order models were found consistent with the numerical results of the full network. An analytical treatment for the stability of the reduced-order model for two subpopulations is derived, which is in good agreement with the numerical simulations. The coupling has a significant role in changing the dynamics of the network for different parameter sets. The network converges to a quiescent state when we increase the number of excitable neurons in the network. This suggests that there is a push–pull effect between the clusters. The oscillatory clusters tried to push up the quiescent state towards oscillatory states and vice versa [60].

Ethics. This work involves only mathematical ideas with biophysical models and computer simulations.

Data accessibility. All the source codes are available at http://modeldb.yale.edu/264594.

Authors' contributions. A.M. and C.H. designed the research work. A.M., C.H. and S.K.S. analysed the results. A.M., S.K.S. and A.M. (Arnab Mondal) performed the analytical results and numerical

Downloaded from https://royalsocietypublishing.org/ on 23 May 2022

results. A.M., S.K.S., R.K.U. and C.H. wrote the manuscript. R.K.U. supported with constructive suggestions.

Competing interests. We declare we have no competing interests.

Funding. This work is supported by University Grants Commission (UGC), Govt. of India under NET-JRF scheme to S.K.S. and the Council of Scientific and Industrial Research (CSIR), Govt. of India under grant no. 25(0277)/17/EMR-II to R.K.U. C.H. is supported by DST-INSPIRE Faculty grant no. IFA17-PH193.

Acknowledgements. The authors are thankful to Dr Wondimu W. Teka (Researcher, U.S. Food and Drug Administration, Washington, DC, USA) for his suggestions and numerical support.

Appendix A

The Jacobian matrix of the fractional-order L-H interneuron model is given by

$$J = \begin{pmatrix} a_{11} & a_{12} & a_{13} \\ a_{21} & a_{22} & a_{23} \\ a_{31} & a_{32} & a_{33} \end{pmatrix},$$

where the coefficients at the fixed point ($v^*,\ h^*,\ m^*$) are given as follows:

$$a_{11} = -60(m^*)^2 - 16 - 400\left(\frac{1}{1+e^{a_1(b_1+v^*)}}\right)^3 h^* - 180\,000\left(\frac{1}{1+e^{a_1(b_1+v^*)}}\right)^4 e^{a_1(b_1+v^*)} h^*(v^* - 0.045),$$

$$a_{12} = -400\left(\frac{1}{1+e^{a_1(b_1+v^*)}}\right)^3 (v^* - 0.045),$$

$$a_{13} = -120m^*(v^* + 0.07),$$

$$a_{21} = -12345\left(\frac{1}{1+e^{a_2(b_2+v^*)}}\right)^2 e^{a_2(b_2+v^*)},$$

$$a_{22} = -24.69, \quad a_{23} = 0$$

and $$a_{31} = 332\left(\frac{1}{1+e^{a_3(b_3+V_{K2}^{\text{shift}}+v^*)}}\right)^2 e^{a_3(b_3+V_{K2}^{\text{shift}}+v^*)},$$

$$a_{32} = 0, \quad a_{33} = -4.$$

Appendix B

The three fractional L-H oscillators representing the entire network (for three population $p+q+r=N$) described in (5.1)

$$\begin{aligned}
\frac{d^\alpha v_\alpha}{dt^\alpha} &= -2[30{m_\alpha}^2(v_\alpha + 0.07) + 8(v_\alpha + 0.046) + 200h(v_\alpha - 0.045)g^3(a_1,\ b_1,\ v_\alpha)] + \frac{D}{N}(q(v_\beta - v_\alpha) + r(v_\gamma - v_\alpha)),\\
\frac{d^\alpha h_\alpha}{dt^\alpha} &= 24.69[g(a_2,\ b_2,\ v_\alpha) - h_\alpha],\\
\frac{d^\alpha m_\alpha}{dt^\alpha} &= 4[g(a_3,\ b_3 + V_{K2}^{\text{shift}},\ v_\alpha) - m_\alpha],\\
\frac{d^\beta v_\beta}{dt^\beta} &= -2[30{m_\beta}^2(v_\beta + 0.07) + 8(v_\beta + 0.046) + 200h(v_\beta - 0.045)g^3(a_1,\ b_1,\ v_\beta)] + \frac{D}{N}(p(v_\alpha - v_\beta) + r(v_\gamma - v_\beta)),\\
\frac{d^\beta h_\beta}{dt^\beta} &= 24.69[g(a_2,\ b_2,\ v_\beta) - h_\beta],\\
\frac{d^\beta m_\beta}{dt^\beta} &= 4[g(a_3,\ b_3 + V_{K2}^{\text{shift}},\ v_\beta) - m_\beta],\\
\frac{d^\gamma v_\gamma}{dt^\gamma} &= -2[30{m_\gamma}^2(v_\gamma + 0.07) + 8(v_\gamma + 0.046) + 200h(v_\gamma - 0.045)g^3(a_1,\ b_1,\ v_\gamma)] + \frac{D}{N}(p(v_\alpha - v_\gamma) + q(v_\beta - v_\gamma)),\\
\frac{d^\gamma h_\gamma}{dt^\gamma} &= 24.69[g(a_2,\ b_2,\ v_\gamma) - h_\gamma],\\
\frac{d^\gamma m_\gamma}{dt^\gamma} &= 4[g(a_3,\ b_3 + V_{K2}^{\text{shift}},\ v_\gamma) - m_\gamma].
\end{aligned} \tag{B 1}$$

For two populations ($p+q=N$), the last three equations of (B1) and second term in each coupling function will not appear. The state variables $h_{\alpha,\beta,\gamma}$ and $m_{\alpha,\beta,\gamma}$ represent the membrane channel gating variables. $\alpha \in (0,\ 1]$ is the fractional exponent and $g(a_i,\ b_i,\ v_{\alpha,\beta,\gamma}) = 1/(1+e^{a_i(b_i+v_{\alpha,\beta,\gamma})})$, $\forall i = 1, 2, 3$.

References

1. Connors BW, Gutnick MJ. 1990 Intrinsic firing patterns of diverse neocortical neurons. *Trends Neurosci.* **13**, 99–104. (doi:10.1016/0166-2236(90)90185-D)
2. Dupont G, Falcke M, Kirk V, Sneyd J. 2016 Neurons and other excitable cells. In *Models of calcium signalling* (eds S Antman, L Greengard, PJ Holmes), pp. 337–385. Berlin, Germany: Springer.
3. Izhikevich EM. 2004 Which model to use for cortical spiking neurons? *IEEE Trans. Neural. Netw.* **15**, 1063–1070. (doi:10.1109/TNN.2004.832719)
4. Izhikevich EM. 2003 Simple model of spiking neurons. *IEEE Trans. Neural Netw.* **14**, 1569–1572. (doi:doi.10.1109/TNN.2003.820440)
5. Izhikevich EM. 2000 Neural excitability, spiking and bursting. *Int. J. Bifurc. Chaos* **10**, 1171–1266. (doi:10.1142/S0218127400000840)
6. Izhikevich EM. 2007 *Dynamical systems in neuroscience*. Cambridge, MA: MIT Press.
7. Ghosh S, Mondal A, Ji P, Mishra A, Dana SK, Antonopoulos CG, Hens C. 2020 Emergence of mixed mode oscillations in random networks of diverse excitable neurons: the role of neighbors and electrical coupling. *Front. Comput. Neurosci.* **14**, 1–49. (doi:10.3389/fncom.2020.00049)
8. Oldham K, Spanier J. 1974 *The fractional calculus theory and applications of differentiation and integration to arbitrary order*. Amsterdam, The Netherlands: Elsevier.
9. Podlubny I. 1998 *Fractional differential equations: an introduction to fractional derivatives, fractional differential equations, to methods of their solution and some of their applications*. Amsterdam, The Netherlands: Elsevier.
10. Podlubny I. 2002 Geometric and physical interpretation of fractional integration and fractional differentiation. *Fract. Calc. Appl. Anal.* **5**, 367–386.
11. Magin RL. 2004 Fractional calculus in bioengineering, Part 1. *Crit. Rev. Biomed. Eng.* **32**, 1104. (doi10.1615/CritRevBiomedEng.v32.i1.10)
12. Zhou Y, Ionescu C, Machado JAT. 2015 Fractional dynamics and its applications. *Nonlinear Dyn.* **80**, 1661–1664. (doi:10.1007/s11071-015-2069-2)
13. Mondal A, Sharma SK, Upadhyay RK, Mondal A. 2019 Firing activities of a fractional-order FitzHugh–Rinzel bursting neuron model and its coupled dynamics. *Sci. Rep.* **9**, 1–11. (doi:10.1038/s41598-019-52061-4)
14. Shi M, Wang Z. 2014 Abundant bursting patterns of a fractional-order Morris–Lecar

Downloaded from https://royalsocietypublishing.org/ on 23 May 2022

neuron model. *Commun. Nonlinear Sci. Numer. Simul.* **19**, 1956–1969. (doi:10.1016/j.cnsns.2013.10.032)

15. Weinberg SH. 2015 Membrane capacitive memory alters spiking in neurons described by the fractional-order Hodgkin–Huxley model. *PLoS ONE* **10**, e0126629. (doi:10.1371/journal.pone.0126629)
16. Mondal A, Upadhyay RK. 2018 Diverse neuronal responses of a fractional-order Izhikevich model: journey from chattering to fast spiking. *Nonlinear Dyn.* **91**, 1275–1288. (doi:10.1007/s11071-017-3944-9)
17. Teka WW, Upadhyay RK, Mondal A. 2018 Spiking and bursting patterns of fractional-order Izhikevich model. *Commun. Nonlinear Sci. Numer. Simul.* **56**, 161–176. (doi:10.1016/j.cnsns.2017.07.026)
18. Teka WW, Upadhyay RK, Mondal A. 2017 Fractional-order leaky integrate-and-fire model with long-term memory and power law dynamics. *Neural Netw.* **93**, 110–125. (doi:10.1016/j.neunet.2017.05.007)
19. Lundstrom BN, Higgs MH, Spain WJ, Fairhall AL. 2008 Fractional differentiation by neocortical pyramidal neurons. *Nat. Neurosci.* **11**, 1335–1342. (doi:10.1038/nn.2212)
20. Teka W, Marinov TM, Santamaria F. 2014 Neuronal spike timing adaptation described with a fractional leaky integrate-and-fire model. *PLoS Comput. Biol.* **10**, e1003526. (doi:10.1371/journal.pcbi.1003526)
21. Teka W, Stockton D, Santamaria F. 2016 Power-law dynamics of membrane conductances increase spiking diversity in a Hodgkin–Huxley model. *PLoS Comput. Biol.* **12**, e1004776. (doi:10.1371/journal.pcbi.1004776)
22. Du M, Wang Z, Hu H. 2013 Measuring memory with the order of fractional derivative. *Sci. Rep.* **3**, 3431. (doi:10.1038/srep03431)
23. Machado JT, Pinto CMA, Lopes AM. 2015 A review on the characterization of signals and systems by power law distributions. *Signal Process* **107**, 246–253. (doi:10.1016/j.sigpro.2014.03.003)
24. Magin RL. 2010 Fractional calculus models of complex dynamics in biological tissues. *Comput. Math. Appl.* **59**, 1586–1593. (doi:10.1016/j.camwa.2009.08.039)
25. Oldham KB, Spanier J. 2006 *The fractional calculus: theory and applications of differentiation and integration to arbitrary order*. New York, NY: Dover.
26. Magin RL, Ovadia M. 2008 Modeling the cardiac tissue electrode interface using fractional calculus. *J. Vib. Control* **14**, 1431–1442. (doi:10.1177/1077546307087439)
27. Goychuk I, Hnggi P. 2004 Fractional diffusion modeling of ion channel gating. *Phys. Rev. E* **70**, 051915. (doi:10.1103/PhysRevE.70.051915)
28. Sierociuk D, Dzieliński A, Sarwas G, Petras I, Podlubny I, Skovranek T. 2013 Modelling heat transfer in heterogeneous media using fractional calculus. *Phil. Trans. R. Soc. A* **371**, 20120146. (doi:10.1098/rsta.2012.0146)
29. Hanyga A, Magin RL. 2014 A new anisotropic fractional model of diffusion suitable for applications of diffusion tensor imaging in biological tissues. *Proc. R. Soc. A* **470**, 20140319. (doi:10.1098/rspa.2014.0319)
30. Sierociuk D, Skovranek T, Macias M, Podlubny I, Petras I, Dzielinski A, Ziubinski P. 2015 Diffusion process modeling by using fractional-order models. *Appl. Math. Comput.* **257**, 2–11. (doi:10.1016/j.amc.2014.11.028)
31. Madhukar A, Park Y, Kim W, Sunaryanto HJ, Berlin R, Chamorro LP, Bentsman J, Ostoja-Starzewski M. 2019 Heat conduction in porcine muscle, blood: experiments and time-fractional telegraph equation model. *J. R. Soc. Interface* **16**, 20190726. (doi:10.1098/rsif.2019.0726)
32. ueno-Orovio A, Kay D, Grau V, Rodriguez B, Burrage K. 2014 Fractional diffusion models of cardiac electrical propagation: role of structural heterogeneity in dispersion of repolarization. *J. R. Soc. Interface* **11**, 20140352. (doi:10.1098/rsif.2014.0352)
33. Kaslik E, Sivasundaram S. 2012 Nonlinear dynamics and chaos in fractional-order neural networks. *Neural Netw.* **32**, 245–256. (doi:10.1016/j.neunet.2012.02.030)
34. Anastasio TJ. 1994 The fractional-order dynamics of brainstem vestibulo-oculomotor neurons. *Biol. Cybern.* **72**, 69–79. (doi:10.1007/BF00206239)
35. Donkin C, Nosofsky RM. 2012 A power-law model of psychological memory strength in short-and long-term recognition. *Psychol. Sci.* **23**, 625–634. (doi:10.1177/0956797611430961)
36. Fairhall AL, Lewen GD, Bialek W, de Ruyter Van Steveninck RR. 2001 Multiple timescales of adaptation in a neural code. In *Advances in Neural Information Processing Systems 13 (NIPS 2000)* (eds TK Leen, TG Dietterich, V Tresp), pp. 115–121. See https://papers.nips.cc/paper/1809-multiple-timescales-of-adaptation-in-a-neural-code.pdf.
37. Anastasio TJ. 1998 Nonuniformity in the linear network model of the oculomotor integrator produces approximately fractional-order dynamics and more realistic neuron behavior. *Biol. Cybern.* **79**, 377–391. (doi:10.1007/s004220050487)
38. Upadhyay RK, Mondal A. 2015 Dynamics of fractional-order modified Morris–Lecar neural model. *Netw. Biol.* **5**, 113–136.
39. Kaslik E, Neamtu M. 2016 Stability and Hopf bifurcation analysis for the hypothalamic–pituitary–adrenal axis model with memory. *Math. Med. Biol.* **35**, 49–78. (doi:10.1093/imammb/dqw020)
40. Brandibur O, Kaslik E. 2017 Stability properties of a two-dimensional system involving one Caputo derivative and applications to the investigation of a fractional-order Morris–Lecar neuronal model. *Nonlinear Dyn.* **90**, 2371–2386. (doi:10.1007/s11071-017-3809-2)
41. Brandibur O, Kaslik E. 2018 Stability of two component incommensurate fractional-order systems and applications to the investigation of a FitzHugh–Nagumo neuronal model. *Math. Method Appl. Sci.* **41**, 7182–7194. (doi:10.1002/mma.4768)
42. Kopell N. 1998 *Toward a theory of modelling generators. Neural control of rhythmic movements in vertebrates*. New York, NY: Wiley.
43. Shilnikov A. 2012 Complete dynamical analysis of a neuron model. *Nonlinear Dyn.* **68**, 305–328. (doi:10.1007/s11071-011-0046-y)
44. Bazhenov M, Timofeev I, Steriade M, Sejnowski T. 2000 Spiking-bursting activity in the thalamic reticular nucleus initiates sequences of spindle oscillations in thalamic networks. *J. Neurophysiol.* **84**, 1076–1087. (doi:10.1152/jn.2000.84.2.1076)
45. Kramer MA, Kirsch HE, Szeri AJ. 2005 Pathological pattern formation and cortical propagation of epileptic seizures. *J. R. Soc. Interface* **2**, 113–127. (doi:10.1098/rsif.2004.0028)
46. Dana SK, Sengupta DC, Hu CK. 2006 Spiking and bursting in Josephson junction. *IEEE Trans. Circuits Syst. -II, Express Briefs* **53**, 1031–1034. (doi:10.1109/TCSII.2006.882183)
47. Channell P, Cymbalyuk G, Shilnikov A. 2007 Origin of bursting through homoclinic spike adding in a neuron model. *Phys. Rev. Lett.* **98**, 134101. (doi:10.1103/PhysRevLett.98.134101)
48. Shilnikov A, Calabrese RL, Cymbalyuk G. 2005 Mechanism of bistability: tonic spiking and bursting in a neuron model. *Phys. Rev. E* **71**, 056214. (doi:10.1103/PhysRevE.71.056214)
49. Adhikari BM, Prasad A, Dhamala M. 2011 Time-delay-induced phase-transition to synchrony in coupled bursting neurons. *Chaos* **21**, 023116. (doi:10.1063/1.3584822)
50. Cymbalyuk G, Shilnikov A. 2005 Coexistence of tonic spiking oscillations in a leech neuron model. *J. Comput. Neurosci.* **18**, 255–263. (doi:10.1007/s10827-005-0354-7)
51. Tavazoei M S, Haeri M. 2008 Chaotic attractors in incommensurate fractional order systems. *Physica D* **237**, 2628–2637. (doi:10.1016/j.physd.2008.03.037)
52. Lenka BK, Banerjee S. 2018 Sufficient conditions for asymptotic stability and stabilization of autonomous fractional order systems. *Commun. Nonlinear Sci. Numer. Simul.* **56**, 365–379. (doi:10.1016/j.cnsns.2017.08.005)
53. Ahmed E, El-Sayed AMA, El-Saka HA. 2006 On some Routh–Hurwitz conditions for fractional-order differential equations and their applications in Lorenz, Rössler, Chua and Chen systems. *Phys. Lett. A* **358**, 1–4. (doi:10.1016/j.physleta.2006.04.087)
54. Tavazoei MS, Haeri M. 2007 A necessary condition for double scroll attractor existence in fractional-order systems. *Phys. Lett. A* **367**, 102–113. (doi:10.1016/j.physleta.2007.05.081)
55. Muthukumar P, Balasubramaniam P, Ratnavelu K. 2014 Synchronization and an application of a novel fractional-order king cobra chaotic system. *Chaos* **24**, 033105. (doi:10.1063/1.4886355)
56. Tavazoei MS, Haeri M. 2009 A note on the stability of fractional-order systems. *Math. Comput. Simul.* **79**, 1566–1576. (doi:10.1016/j.matcom.2008.07.003)

57. Dhooge A, Govaerts W, Kuznetsov YA, Meijer HGE, Sautois B. 2008 New features of the software MatCont for bifurcation analysis of dynamical systems. *Math. Comp. Modell. Dyn. Syst.* **14**, 147–175. (doi:10.1080/13873950701742754)
58. Upadhyay RK, Mondal A, Teka WW. 2017 Fractional-order excitable neural system with bidirectional coupling. *Nonlinear Dyn.* **87**, 2219–2233. (doi:10.1007/s11071-016-3185-3)
59. Zhang F, Chen G, Li C, Kurths J. 2013 Chaos synchronization in fractional differential systems. *Phil. Trans. R. Soc. A* **371**, 20120155. (doi:10.1098/rsta.2012.0155)
60. Hens C, Pal P, Dana S. 2015 Bursting dynamics in a population of oscillatory and excitable Josephson junctions. *Phys. Rev. E* **92**, 022915. (doi:10.1103/PhysRevE.92.022915)
61. Mondal A, Sharma SK, Upadhyay RK, Aziz-Alaoui MA, Kundu P, Hens C. 2019 Diffusion dynamics of a conductance-based neuronal population. *Phys. Rev. E* **99**, 042307. (doi:10.1103/PhysRevE.99.042307)
62. Nandan M, Hens C, Pal P, Dana S. 2014 Transition from amplitude to oscillation death in a network of oscillators. *Chaos* **24**, 043103. (doi:10.1063/1.4897446)
63. Pazó D, Montbrió E. 2006 Universal behavior in populations composed of excitable and self-oscillatory elements. *Phys. Rev. E* **73**, 055202. (doi:10.1103/PhysRevE.73.055202)

Downloaded from https://royalsocietypublishing.org/ on 23 May 2022